Int. J. Appl. Math. Comput. Sci., 2023, Vol. 33, No. 1, 33–43
DOI: 10.34768/amcs-2023-0003

INFRARED SMALL–TARGET DETECTION UNDER A COMPLEX BACKGROUND BASED ON A LOCAL GRADIENT CONTRAST METHOD

LINNA YANG [a,*], TAO XIE [a], MINGXING LIU [a], MINGJIANG ZHANG [a], SHUAIHUI QI [a], JUNGANG YANG [a]

[a] College of Information and Communication
National University of Defense Technology
No. 618 Yanhe Avenue, Qiaokou District, 430030 Wuhan City, China
e-mail: yanglinna@nudt.edu.cn

Small target detection under a complex background has always been a hot and difficult problem in the field of image processing. Due to the factors such as a complex background and a low signal-to-noise ratio, the existing methods cannot robustly detect targets submerged in strong clutter and noise. In this paper, a local gradient contrast method (LGCM) is proposed. Firstly, the optimal scale for each pixel is obtained by calculating a multiscale salient map. Then, a subblock-based local gradient measure is designed; it can suppress strong clutter interference and pixel-sized noise simultaneously. Thirdly, the subblock-based local gradient measure and the salient map are utilized to construct the LGCM. Finally, an adaptive threshold is employed to extract the final detection result. Experimental results on six datasets demonstrate that the proposed method can discard clutters and yield superior results compared with state-of-the-art methods.

Keywords: small target detection, local gradient contrast, visual saliency, infrared image processing.

1. Introduction

Small target detection has been widely applied in the fields of intelligent visual observation systems (Yao *et al*., 2022; Baran *et al*., 2016; Chmiel *et al*., 2016), early warning systems (Li *et al*., 2021), infrared (IR) image information processing (Yang *et al*., 2022) and target detection (Uzair *et al*., 2020; Tabor, 2010). Due to the long detection distance, the target occupies few pixels in the infrared image and lacks the shape and geometric characteristics. Additionally, the complex and varied background environment and the low signal-to-noise ratio make it difficult to detect real targets (Han *et al*., 2018b; Yu *et al*., 2022).

In the human visual system (HVS), researchers utilize the visual attention mechanism to identify the most salient areas in the image (Liu *et al*., 2018a; Han *et al*., 2019; Kowalski *et al*., 2014) and use a salient map to indicate this significance (Andrysiak and Choras, 2005; Xie *et al*., 2018). The target detection algorithms based on the HVS mechanism show robust capabilities in the signal-to-noise ratio improvement, background clutter suppression and noise suppression. The local contrast method (LCM) (Chen *et al*., 2014) exploits the HVS to enhance the targets by calculating the contrast between the central subblock and the surrounding subblocks, which produces encouraging results. The relative local contrast measure (RLCM) (Han *et al*., 2018a) makes real targets prominent and suppresses all the types of interferences simultaneously. The accelerated multiscale weighted local contrast measure (AMWLCM) (Liu *et al*., 2018b) not only takes advantage of the local contrast of the target and the consistency of the background, but also takes into account the imaging characteristics of the clutter edges, which greatly reduces false alarms.

The multiscale local contrast measure using a local energy factor (MLCM-LEF) (Xia *et al*., 2020) measures the local contrast from two aspects: the local dissimilarity and the local brightness difference. Aghaziyarati *et al*. (2019) compensate the average absolute gray difference (AAGD) (Deng *et al*., 2016) disadvantages using cumulative directional derivatives. The multiscale patch-based contrast measure (MPCM)

*Corresponding author

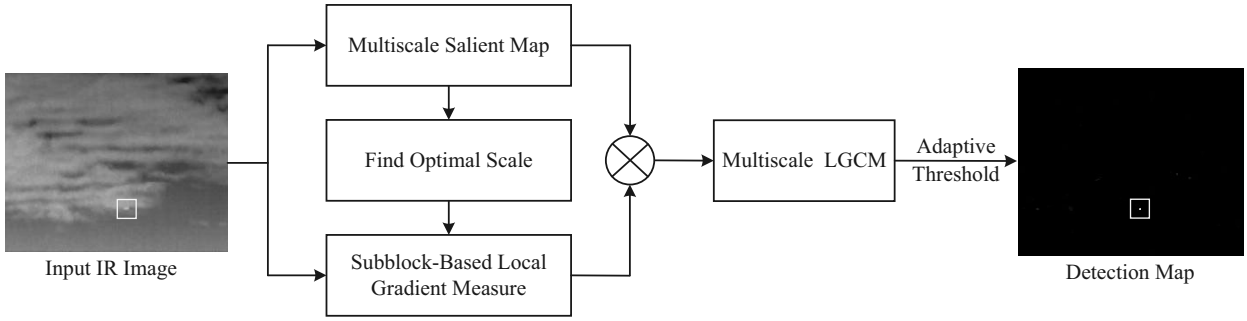

Fig. 1. Flowchart of the proposed method.

(Wei *et al*., 2016) can increase the contrast between the target and the background, which makes it easy to segment a small target by simple adaptive thresholding method. The high-boost-based multiscale local contrast measure (HBMLCM) (Shi *et al*., 2018) proposed a high boost filter to enhance the high frequency signal where the target may appear and suppress the low frequency signal. Li *et al*. (2019) combine the dual-window local contrast method (DW-LCM) and the multiscale window IR patch-image (MW-IPI) together, exploiting both local and nonlocal priors. A local contrast measure based on infrared gradient vector field (IGVF) features is employed in the local gradient field feature contrast measure (LGFFCM) Xiong *et al*. (2021).

In addition to the contrast mechanism, many other properties (Zhang *et al*., 2019) can be used to enhance the targets and discard clutters. Gradients, for instance, can be utilized to enhance the contours and edges of objects in the image. The local intensity and gradient (LIG) (Zhang *et al*., 2018) can yield a target enhancement and clutter suppression by calculating the local intensity and gradient of the original infrared image. A difference between the variances of the layers (Nasiri and Chehresa, 2017) in the neighboring areas can also lead to effective detection results.

However, it is still a challenge to robustly extract small targets from a complex background with strong clutter interference. In this paper, a subblock-based local gradient measure is innovatively designed. It can suppress strong clutter and pixel-sized noise simultaneously. Then, a multiscale local gradient contrast method (LGCM) is calculated from the subblock-based local gradient measure; it can deal with different sizes of small targets and achieve a favorable detection performance.

2. Methods

The flowchart of the proposed method is shown in Fig. 1. First, the optimal scale is obtained by a multiscale salient map. Then the subblock-based local gradient measure is calculated with the optimal scale. Thirdly, the multiscale LGCM is constructed utilizing the subblock-based local gradient measure and salient map. Finally, an adaptive threshold is applied to extract small targets.

2.1. Construction of the subblock-based local gradient measure. The input IR image can be regarded as a two-dimensional discrete function. The image gradient is actually the derivative of this two-dimensional discrete function. The image gradient G is commonly defined as

$$G(i,j) = d_x(i,j) + d_y(i,j), \tag{1}$$

$$d_x(i,j) = I(i+1,j) - I(i,j), \tag{2}$$

$$d_y(i,j) = I(i,j+1) - I(i,j), \tag{3}$$

where $I(i,j)$ is the gray value of the pixel (i,j), $d_x(i,j)$ and $d_y(i,j)$ are the gradients in the x and y directions, respectively.

The gradients of the targets exhibit isotropic Gaussian characteristics, while the gradients of the clutters with edges are generally consistent. Therefore, the gradient characteristics can be integrated into the small target detection to discard the clutter of edges.

For target (presented in Fig. 2(b), its gradient value is relatively large, and almost all gradient vectors point to its center. For the background with edges (presented in Fig. 2(c)), although the gradient value is also large, the direction is usually locally orientated. For the smooth background, the gradient value is relatively small and messy.

The gradients obtained by (1)–(3) can be very sensitive to differences between adjacent pixels, and have a good positioning of edges and contours, but this pixel-based gradient calculation is quite sensitive to noise. In the pursuit of small target detection under a complex background, pixel-based gradient calculation can easily misinterpret noise as a target and give a false alarm. Therefore, the pixel-based gradient calculation method is extended to subblock-based gradient calculation in this paper, and a subblock-based local gradient measure is

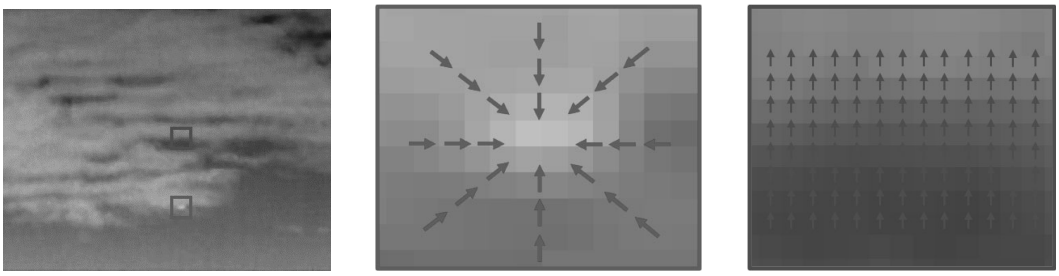

(a) (b) (c)

Fig. 2. Gradient direction: original IR image with two squares (a), gradient direction of the target (zooming in on the lower square) (b), gradient direction of the edges (zooming in on the upper square) (c).

proposed that fully utilizes the gradient characteristics of small targets.

The specific calculations of the subblock-based local gradient measure are as follows. Employing a sliding window w (its size is $3p \times 3p$) move on the image from left to right, top to bottom (as shown in Fig. 3(a)). Then the sliding window w is divided into 9 subblocks on the average, each subblock is recorded as $B0, \ldots, B8$ (as shown in Fig. 3(b)).

For each pixel, its gradient value $\varphi(i,j)$ consists of eight components coming from eight directions. The gradient value in each direction $\varphi_n(i,j), n = 1, \ldots, 8$ is the gray value difference between its center subblock B_0 and its surrounding subblock $B_n (n = 1, \ldots, 8)$.

$$\varphi(i,j) = [\varphi_1(i,j), \varphi_2(i,j), \ldots, \varphi_8(i,j)], \quad (4)$$

$$\varphi_n(i,j) = I_{B0} - I_{Bn}, \quad n = 1, \ldots, 8, \quad (5)$$

$$\varphi_n(i,j) = \max(\varphi_n(i,j), 0), \quad n = 1, \ldots, 8. \quad (6)$$

Here $I_{B0}, \ldots, I_{B8}$ are the mean gray value of subblocks $B_0, \ldots, B_8$. The gray value of the target subblock should be greater than the gray values of the surrounding subblocks. Thus, removing the value of $\varphi_n(i,j) < 0$ can effectively suppress the interference of clutter and noise.

Then calculate the maximum and minimum values of $\varphi_n(i,j)$:

$$G_{\max}(i,j) = \max_{n=1}^{8}(\varphi_n(i,j)), \quad (7)$$

$$G_{\min}(i,j) = \min_{n=1}^{8}(\varphi_n(i,j)). \quad (8)$$

The subblock-based local gradient measure is defined as the mean square of $\varphi_n(i,j)$, which can be calculated by the following formula:

$$G(i,j) = \begin{cases} \dfrac{1}{8}\displaystyle\sum_{n=1}^{8} \varphi_n^2(i,j), & \dfrac{G_{\min}(i,j)}{G_{\max}(i,j)} > \lambda, \\ 0, & \text{otherwise}, \end{cases} \quad (9)$$

where λ is a constant from the interval $(0,1)$ obtained from experiments. In this paper, λ takes a value of 0.2.

The effectiveness of the proposed subblock-based local gradient measure is discussed as follows:

1. If pixel (i,j) is a target pixel, then $I_{B0} > I_{Bn}$, $\varphi_n(i,j)$ has a relatively large positive value, $G_{\min}(i,j) \approx G_{\max}(i,j)$, and consequently, its value of $G(i,j)$ is relatively large. Therefore, the target pixel is enhanced.

2. If pixel (i,j) is an edge pixel, its gradient components in different; directions are quite different thus $G_{\min}(i,j) < \lambda \cdot G_{\max}(i,j)$ and then $G(i,j)$ is zero. Therefore, many edge pixels are discarded. Of course, in order not to miss any target, the value of λ will not be large, some edge points will have the value of $G(i,j)$, but its gradient component in each direction will not be greater than the gradient component of the target point, so that the value $G(i,j)$ of edges will be smaller than the value $G(i,j)$ of the target. In this way, it will be eliminated in the subsequent screening.

3. If pixel (i,j) is a strong noise point, its single-point gray value may be as large as that for the target, and the difference with respect to surrounding points is also relatively large, but in this paper subblocks are utilized as the basic units for calculation. After the mean calculation of the whole subblock, the value of I_{B0} is rarely affected by the single-point noise; thus, the strong noise point can also be suppressed.

4. If pixel (i,j) is a gently changing background, then $I_{B0} \approx I_{Bn}$ and both $\varphi_n(i,j)$ and $G(i,j)$ will be very small.

In the above introduction of the subblock-based local gradient measure, every value is calculated based on the pixel (i,j). But in practice, calculating all these formulas pixel by pixel (using the `for` loop) is inefficient and time-consuming. It is recommended to calculate each value based on the whole map. For an IR image with size $m \times n$, when calculating the mean gray value of each subblock, we calculate maps $I_{B0}, \ldots, I_{B8}$. Map I_{B0}, for

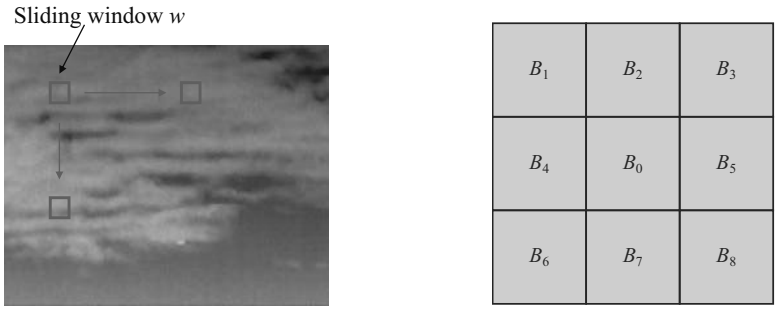

Fig. 3. Sliding window w (its size is $3p \times 3p$): movement of sliding window w (a), subblocks in sliding window w (b).

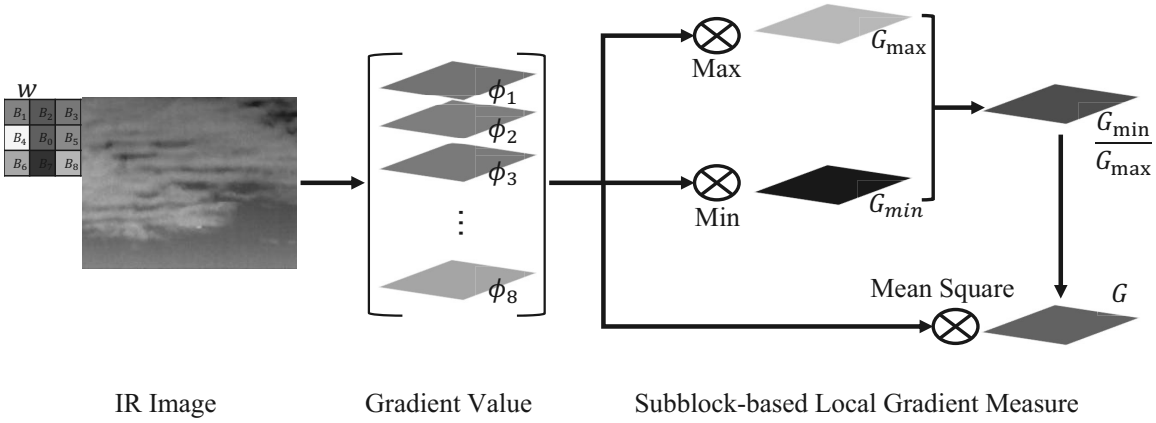

Fig. 4. Flowchart of the subblock-based local gradient measure.

instance, has a size of $m \times n$ and each point in it is the I_{B0} value of the current pixel. In the same way, we can realize parallel processing and make the algorithm more efficient.

Based on this idea, the corresponding flowchart of the subblock-based local gradient measure is shown in Fig. 4.

2.2. Multiscale LGCM calculation. In the previous description, the size of the window w is $3p \times 3p$ and the size of each subblock in the window w is $p \times p$. For each pixel (i, j), different p leads to different $G(i, j)$. In the ideal case, the closer the size of subblock p is to the target size, the larger the gradient value and the larger $G(i, j)$ can be obtained. But in reality, the target size is usually unknown, and in the same image, targets of different sizes may appear. Thus, a multiscale LGCM is necessary.

Firstly, inspired by the RLCM (Han *et al.*, 2018a), the salient map of image I is calculated as

$$P = \min_{n=1}^{8} \left(\frac{I_{B0}}{I_{Bn}} I_{B0} - I_{B0} \right). \tag{10}$$

$I_{B0}, \ldots, I_{B8}$ are the mean gray values of subblocks $B0, \ldots, B8$, respectively, which are the same as defined previously.

The salient map is commonly exploited in the target detection method utilizing a human vision system. It can significantly improve the signal-to-noise ratio of the target and discard noise by calculating the contrast between the central subblock and surrounding subblocks.

For the s-th scale ($s = 1, \ldots, L$, where L is the number of scales been used), calculate its salient map P_s. Then select the maximum $P_s(i, j)$ for each pixel (i, j) as the value of the multiscale salient map $P_{\text{ms}}(i, j)$, and record the scale $s_P(i, j)$ that maximizes the value of $P_{\text{ms}}(i, j)$:

$$P_{\text{ms}}(i, j) = \max_{s=1}^{L} (P_s(i, j)). \tag{11}$$

According to the definition of the Society of Photo-optical Instrumentation Engineers (SPIE), an infrared target with an area not larger than 9×9 is called an infrared small target (Zhang *et al.*, 2003); thus L is usually not too large. In this paper, the value of L is 4, when the values of $scale$ are 1, 2, 3 and 4, and those of p are 3, 5 ,7 and 9.

Then, for the s-th scale, calculate its subblock-based local gradient measure $G(i, j)$. Since the optimal scale for each local area generally corresponds to the local maximum salient map, the value of the multiscale

Table 1. Dataset information.

Dataset	Size	Description
Dataset 1	128×128	comparatively smooth sky background with heavy noise
Dataset 2	300×200	weak targets under strong light and heterogenous background
Dataset 3	250×200	heavy sky clutter background with edges
Dataset 4	128×128	complex background with strong clutter blocks
Dataset 5	128×128	targets of different sizes with heavy noise
Dataset 6	200×150	complex changing background with heavy clutters

Table 2. Parameter description for ten methods in the experiments.

Method	Description
MEXMED	window size: 9×9
MLCM-LEF	$\alpha = 0.5$, $h = 0.2$, size of windows: $[1 \times 1, 3 \times 3, 5 \times 5, 7 \times 7, 9 \times 9]$
MPCM	window size: $[3 \times 3, 5 \times 5, 7 \times 7, 9 \times 9]$
AMWLCM	window size: $[3 \times 3, 3 \times 4, 4 \times 3, 4 \times 4, 4 \times 5, 3 \times 5, 5 \times 3, 5 \times 4, 5 \times 5]$
LCM	window size: $[3 \times 3, 5 \times 5, 7 \times 7, 9 \times 9]$
RLCM	$Scale = 3$, $K_1 = [2, 5, 9]$, $K_2 = [4, 9, 16]$
HBMLCM	window size: $[3 \times 3, 5 \times 5, 7 \times 7, 9 \times 9]$
MS-AAGD	internal window sizes: $[3 \times 3, 5 \times 5, 7 \times 7, 9 \times 9]$, external window sizes: 19×19
LIG	$K = 0.2$, $N = 19$
Ours	window size: $[3 \times 3, 5 \times 5, 7 \times 7, 9 \times 9]$

subblock-based local gradient measure is $G(i, j)$ under the optimal scale $s_P(i, j)$ at each pixel (i, j),

$$G_{\text{ms}}(i, j) = G_s(i, j). \tag{12}$$

where scale $s(i, j) = s_P(i, j)$.

Finally, the multiscale LGCM is defined as

$$\text{LGCM} = G_{\text{ms}} \times P_{\text{ms}}. \tag{13}$$

2.3. Thresholding. In the resulting map of LGCM, the target will be the most salient; the it can be detected through a simple threshold (Han *et al.*, 2020). The adapting threshold in this paper is defined as

$$T_h = k \times \mu_{\text{LGCM}}, \tag{14}$$

where μ_{LGCM} is the mean value of nonzero values in the LGCM, k being a constant value.

3. Experiments and a discussion

In this section, six infrared image datasets are utilized to test the performance of the proposed method. The specific datasets information is summarized in Table 1. All the experiments are conducted on a computer equipped with 8 GB memory and a 2.8 GHz Intel i7 processor. The code is implemented in MATLAB R2016a software.

3.1. Detection performance of the LGCM. To illustrate the effectiveness of the proposed method, Figs. 5 and 6 show the original images and detection results of image samples in six datasets. We exploit the same parameter values for all the sequences. All the data in Figs. 5 and 6 are normalized to the range from 0 to 255.

The first and second rows of Figs. 5 and 6 display the representative original images from six datasets as well as their corresponding three-dimensional mesh maps. To get a better view, real targets are highlighted by square boxes. All the images have interferences such as cloud, strong Gaussian noise, trees, a mountain and so on. Targets in some images are even submerged by clutters. All those factors have a great impact on the detection procedure. However, after the calculation of the LGCM, targets with different sizes are all precisely screened out in the third rows of Figs. 5 and 6. Results in the fourth rows of Figs. 5 and 6 reveal that most backgrounds are discarded, and all the targets are enhanced with a greater signal-to-noise ratio.

3.2. Comparison with other methods. The proposed method is compared with other nine methods, including MaxMedian (Deshpande *et al.*, 1999), MLCM-LEF (Xia *et al.*, 2020), MPCM (Wei *et al.*, 2016), AMWLCM (Liu *et al.*, 2018b), LCM (Chen *et al.*, 2014), RLCM (Han *et al.*, 2018a), HBMLCM (Shi *et al.*, 2018), MS-AAGD (Aghaziyarati *et al.*, 2019) and LIG (Zhang *et al.*, 2018). The parameters of these methods are used as these authors' suggestions. The specific parameters of all the methods in the experiments are listed in Table 2.

In order to objectively evaluate the performance of the proposed LGCM method, several commonly used measurement metrics such as the signal-to-clutter ratio

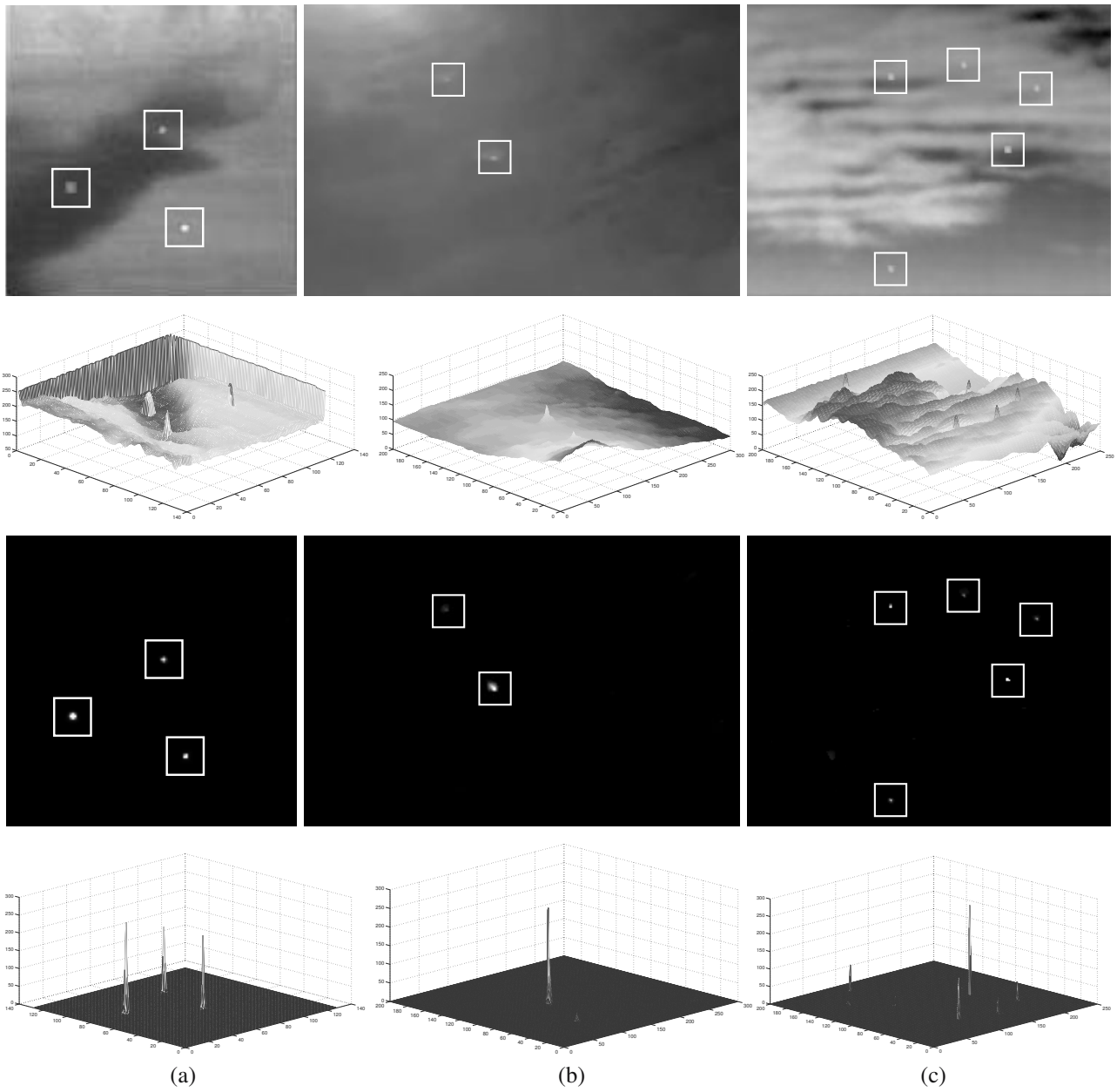

Fig. 5. Original images in the first row, mesh maps for the original images in the second row, detection results in the third row, and mesh maps for the detection results in the fourth row: Dataset 1 (a), Dataset 2 (b), and Dataset 3 (c).

gain (SCRG), background suppression factor (BSF), correct detection probability (PD), false alarm rate (PFA) and average running time are compared in the following. The receiver operating characteristic curve (ROC) represents the varying relationship of the PD and PFA.

Comparison of SNRG and BSF. As a general rule, SNRG determines how much a method has enhanced the target. The higher the BSF in a method, the higher clutter suppression in the result image. In this part, the values of SNRG and BSF of ten methods are compared.

Six images shown in Figs. 5 and 6 are used to calculate the values of SNRG and BSF. For the image with more than one target, the average SCRG and the average BSF are implemented to represent the SNRG and BSF of this image.

In Fig. 7, it can be seen that all the methods can enhance the targets. However, the SNRG values of the proposed method are higher than for most of the methods. It is known that the higher the SNRG, the easier the targets can be detected. It is demonstrated that the proposed method can distinguish targets and the background easily

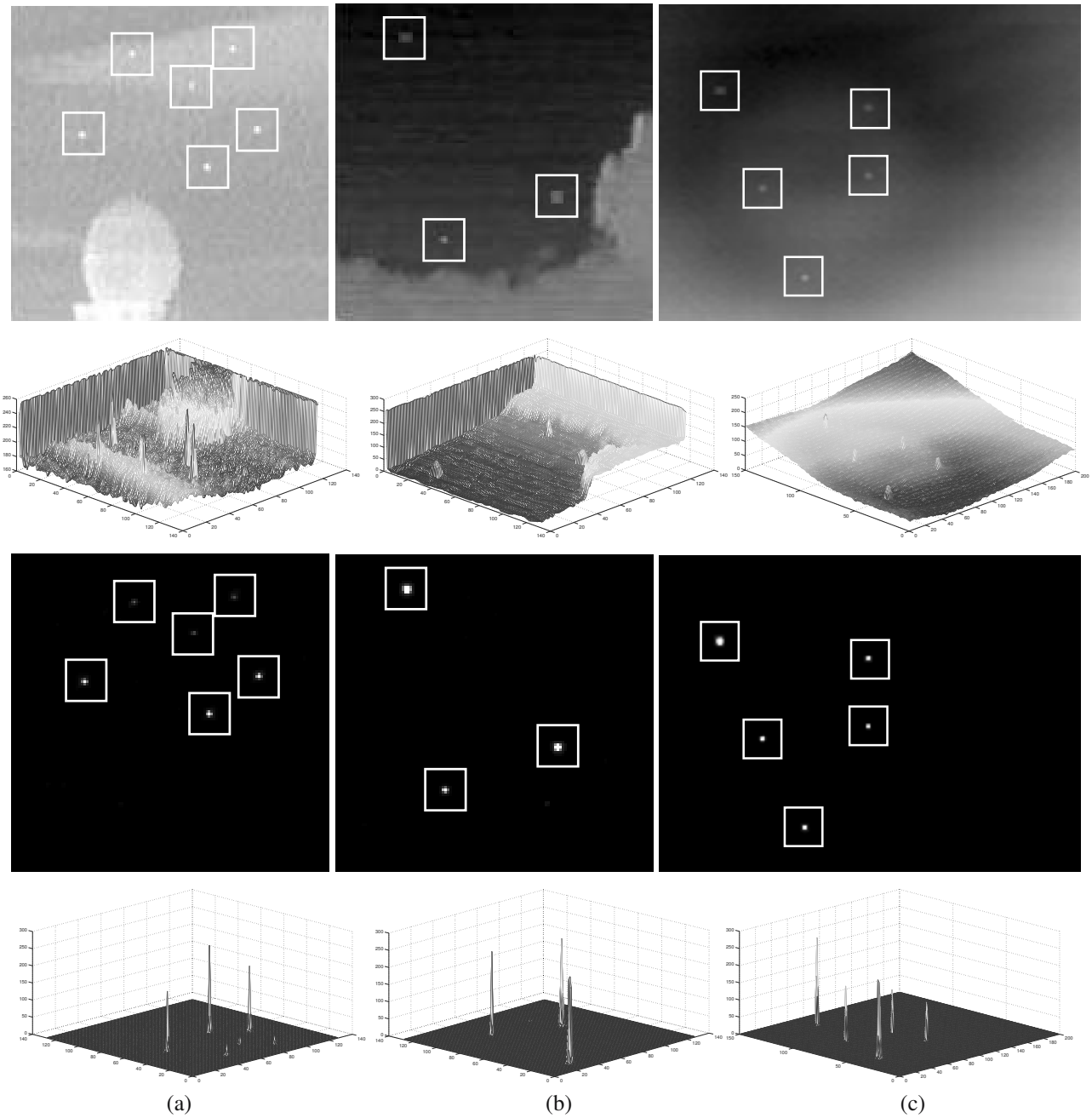

Fig. 6. Original images in the first row, mesh maps for the original images in the second row, detection results in the third row, and mesh maps for the detection results in the fourth row: Dataset 4 (a), Dataset 5 (b), and Dataset 6 (c).

on various scenes.

Noise and background clutter are the sources of false alarms in the small target detection. A good performance on the BSF can effectively reduce the false alarm rate.

In Fig. 8, the values of log(BSF) of the proposed method are far greater than for any other methods. This proves that the proposed method can discard a background with edges, trees, rocks and random noise.

Computation efficiency. As we can see in Fig. 9, the proposed method can achieve striking results with acceptable calculation time. The reasons are as follows.

Firstly, the proposed method is inspired by the RLCM, while it is more efficient than the RLCM, since it omits time-consuming steps of sorting and seeking the maximum value. Secondly, the proposed method calculates each value based on the whole map (as described in detail in Section 2), which makes the method capable of parallel processing.

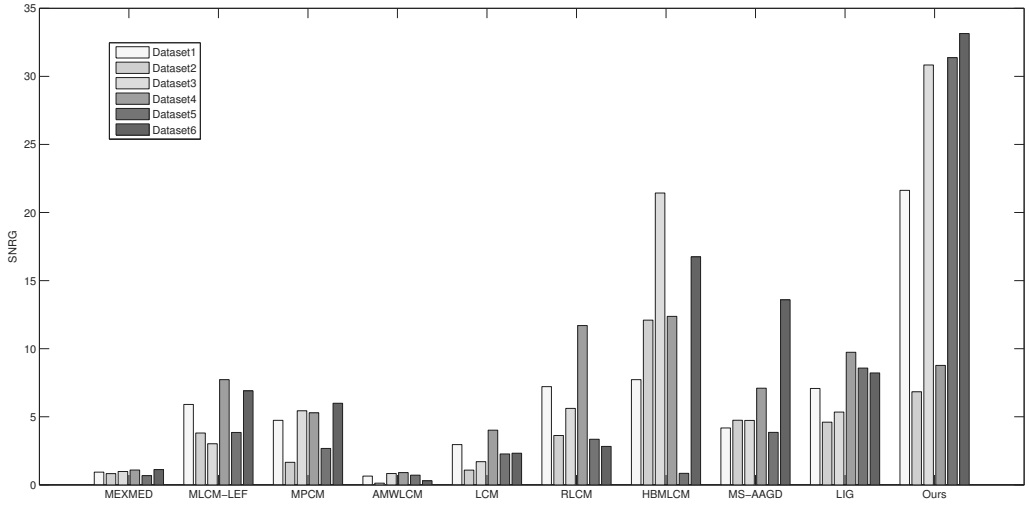

Fig. 7. Bar chart of SNRG.

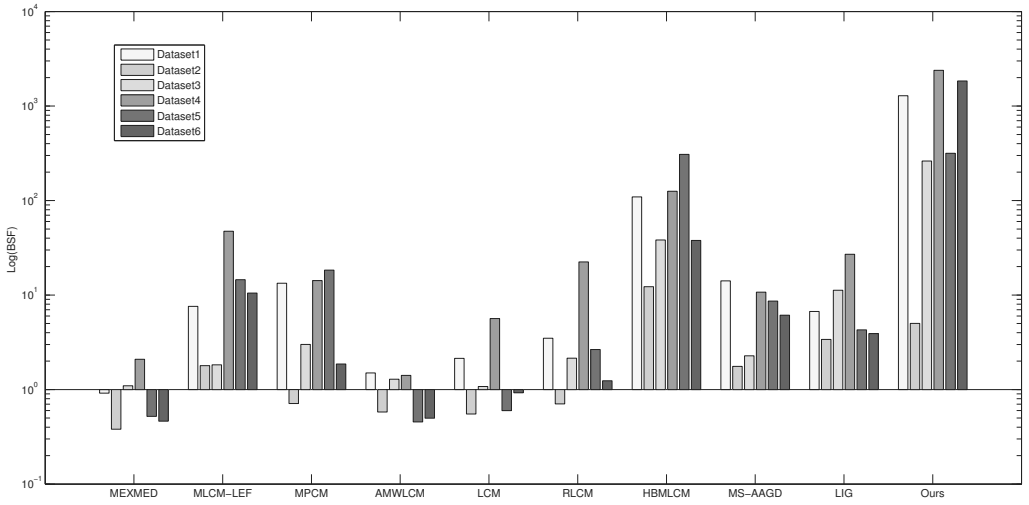

Fig. 8. Bar chart of log(BSF).

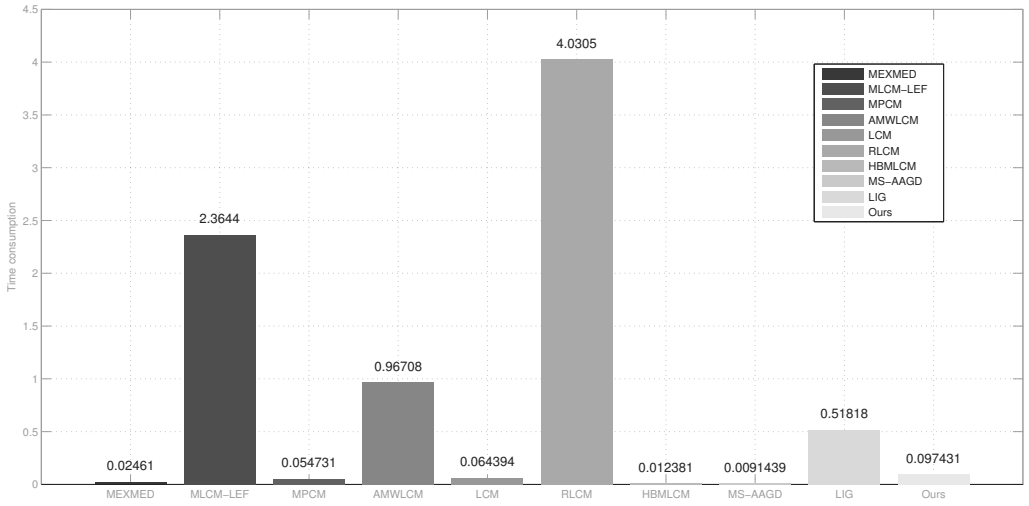

Fig. 9. Time consumption of ten methods (in seconds).

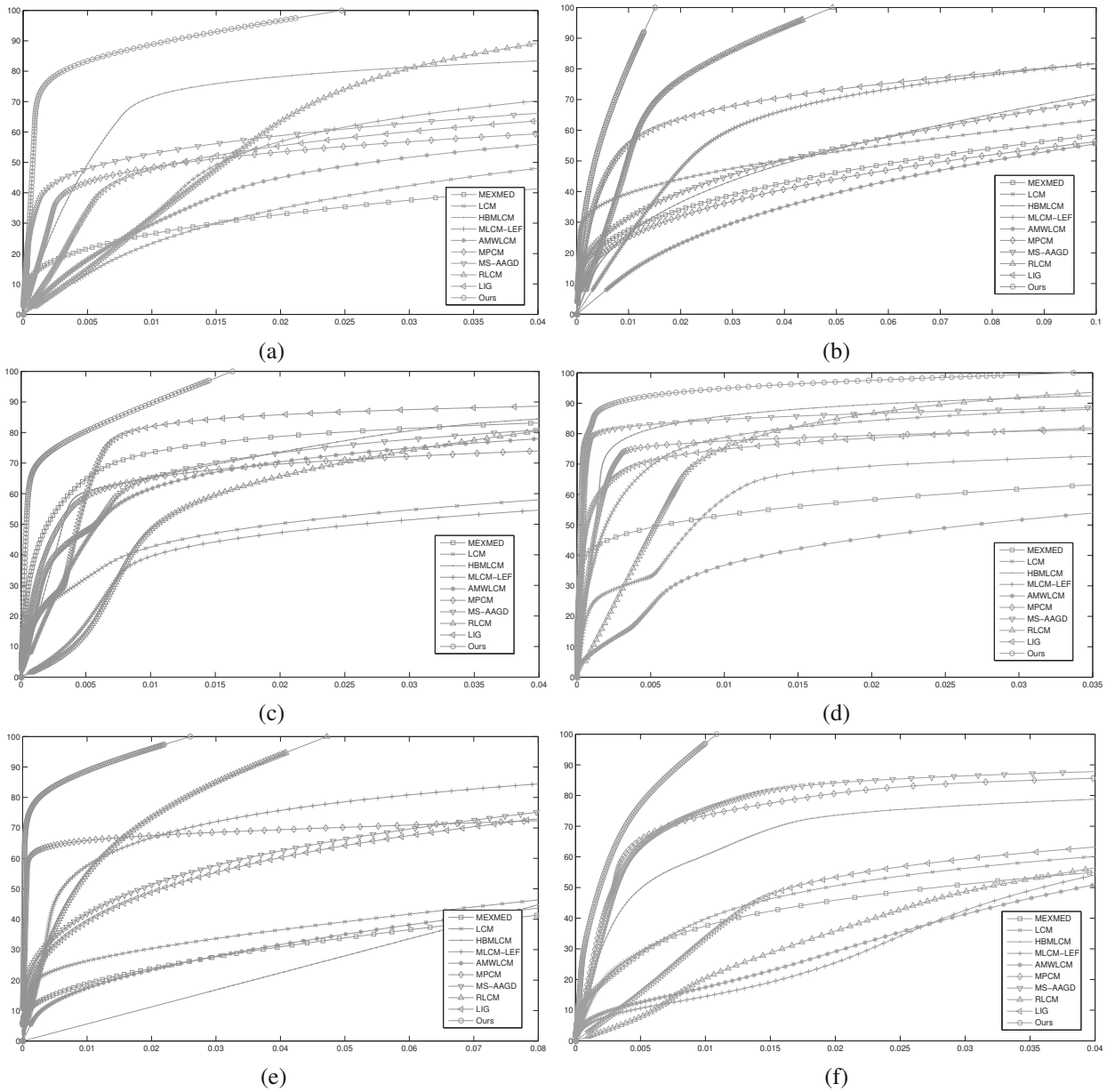

Fig. 10. ROCs for ten methods: Dataset 1 (a), Dataset 2 (b), Dataset 3 (c), Dataset 4 (d), Dataset 5 (e) and Dataset 6 (f).

However, in order to suppress the noise and clutters better, the local gradient and local intensity are utilized in our method, which leads to a slightly longer time consumption than the MEXMED, LCM and several other methods.

Comparison of ROCs. For each dataset, we added random Gaussian noise with the same intensity to every image, and implemented Monte Carlo simulations to get ROC results. The final ROC is obtained by changing the segmentation thresholds for each dataset.

In Fig. 10, compared with other nine baseline methods, the proposed method can achieve the best detection performance with good robustness on all datasets. This is because it can significantly enhance the targets (have bigger SNRG) and discard complex clutters (have bigger BSF).

4. Conclusion

In this paper, a multiscale local gradient contrast method for small target detection under a complex background has been proposed. First, a subblock-based local gradient measure has been designed, which can suppress a complex background with all types of clutter. Then, a multiscale salient map has been obtained to get an optimal scale. Finally, the multiscale LGCM is calculated by exploiting

both the local gradient and local intensity. Experiments on six datasets demonstrate that the proposed method can achieve higher SNRG and BSF values, and exhibit encouraging performance in detection accuracy.

References

Aghaziyarati, S., Moradi, S. and Talebi, H. (2019). Small infrared target detection using absolute average difference weighted by cumulative directional derivatives, *Infrared Physics and Technology* **101**: 78–87, DOI: 10.1016/j.infrared.2019.06.003.

Andrysiak, T. and Choras, M. (2005). Image retrieval based on hierarchical Gabor filters, *International Journal of Applied Mathematics and Computer Science* **15**(4): 471–480.

Baran, R., Rusc, T. and Fornalski, P. (2016). A smart camera for the surveillance of vehicles in intelligent transportation systems, *Multimedia Tools and Applications* **75**(17): 10471–10493, DOI: 10.1007/s11042-015-3151-y.

Chen, C.L.P., Li, H., Wei, Y.T., Xia, T. and Tang, Y.Y. (2014). A local contrast method for small infrared target detection, *IEEE Transactions on Geoscience and Remote Sensing* **52**(1): 574–581, DOI: 10.1109/TGRS.2013.2242477.

Chmiel, W., Danda, J., Dziech, A., Ernst, S., Kadluczka, P., Mikrut, Z., Pawlik, P., Szwed, P. and Wojnicki, I. (2016). Insigma: An intelligent transportation system for urban mobility enhancement, *Multimedia Tools and Applications* **75**(17): 10529–10560, DOI: 10.1007/s11042-016-3367-5.

Deng, H., Sun, X.P., Liu, M.L., Ye, C.H. and Zhou, X. (2016). Infrared small-target detection using multiscale gray difference weighted image entropy, *IEEE Transactions on Aerospace and Electronic Systems* **52**(1): 60–72, DOI: 10.1109/TAES.2015.140878.

Deshpande, S.D., Meng, H.E., Ronda, V. and Chan, P. (1999). Max-mean and max-median filters for detection of small-targets, *Proceedings of SPIE* **3809**: 74–83.

Han, J.H., Liang, K., Zhou, B., Zhu, X.Y., Zhao, J. and Zhao, L.L. (2018a). Infrared small target detection utilizing the multiscale relative local contrast measure, *IEEE Geoscience and Remote Sensing Letters* **15**(4): 612–616, DOI: 10.1109/LGRS.2018.2790909.

Han, J.H., Liu, S.B., Qin, G., Zhao, Q., Zhang, H.H. and Li, N.N. (2019). A local contrast method combined with adaptive background estimation for infrared small target detection, *IEEE Geoscience and Remote Sensing Letters* **16**(9): 1442–1446, DOI: 10.1109/LGRS.2019.2898893.

Han, J.H., Moradi, S., Faramarzi, I., Liu, C.Y., Zhang, H.H. and Zhao, Q. (2020). A local contrast method for infrared small-target detection utilizing a tri-layer window, *IEEE Geoscience and Remote Sensing Letters* **17**(10): 1822–1826, DOI: 10.1109/LGRS.2019.2954578.

Han, J.H., Yu, Y. and Liang, K. (2018b). Infrared small-target detection under complex background based on subblock-level ratio-difference joint local contrast measure, *Optical Engineering* **57**(10): 103105, DOI: 10.1117/1.OE.57.10.103105.

Kowalski, M., Kaczmarek, P., Kabaciński, R., Matuszczak, M., Tranbowicz, K. and Sobkowiak, R. (2014). A simultaneous localization and tracking method for a worm tracking system, *International Journal of Applied Mathematics and Computer Science* **24**(3): 599–609, DOI: 10.2478/amcs-2014-0043.

Li, H., Wang, Q., Wang, H. and Yang, W.K. (2021). Infrared small target detection using tensor based least mean square, *Computers and Electrical Engineering* **91**: 106994, DOI: 10.1016/j.compeleceng.2021.106994.

Li, W., Zhao, M.J., Deng, X.Y., Li, L., Li, L.W. and Zhang, W.J. (2019). Infrared small target detection using local and nonlocal spatial information, *IEEE Journal of Selected Topics in Applied Earth Observations and Remote Sensing* **12**(9): 3677–3689, DOI: 10.1109/JSTARS.2019.2931566.

Liu, J., He, Z.Q., Chen, Z.L. and Shao, L. (2018a). Tiny and dim infrared target detection based on weighted local contrast, *IEEE Geoscience and Remote Sensing Letters* **15**(11): 1780–1784, DOI: 10.1109/LGRS.2018.2856762.

Liu, J., He, Z.Q., Chen, Z.L. and Shao, L. (2018b). Tiny and dim infrared target detection based on weighted local contrast, *IEEE Geoscience and Remote Sensing Letters* **15**(11): 1780–1784, DOI: 10.1109/LGRS.2018.2856762.

Nasiri, M. and Chehresa, S. (2017). Infrared small target enhancement based on variance difference, *Infrared Physics and Technology* **82**: 107–119, DOI: 10.1016/j.infrared.2017.03.003.

Shi, Y.F., Wei, Y.T., Yao, H., Pan, D.H. and Xiao, G.R. (2018). High-boost-based multiscale local contrast measure for infrared small target detection, *IEEE Geoscience and Remote Sensing Letters* **15**(1): 33–37, DOI: 10.1109/LGRS.2017.2772030.

Tabor, Z. (2010). Surrogate data: A novel approach to object detection, *International Journal of Applied Mathematics and Computer Science* **20**(3): 545–553, DOI: 10.2478/v10006-010-0040-4.

Uzair, M., Brinkworth, R.S. and Finn, A. (2020). A bio-inspired spatiotemporal contrast operator for small and low-heat-signature target detection in infrared imagery, *Neural Computing and Applications* **33**(13): 7311–7324, DOI: 10.1007/s00521-020-05206-w.

Wei, Y.T., You, X.G. and Li, H. (2016). Multiscale patch-based contrast measure for small infrared target detection, *Pattern Recognition* **58**: 216–226, DOI: 10.1016/j.patcog.2016.04.002.

Xia, C.Q., Li, X.R., Zhao, L.Y. and Shu, R. (2020). Infrared small target detection based on multiscale local contrast measure using local energy factor, *IEEE Geoscience and Remote Sensing Letters* **17**(1): 157–161, DOI: 10.1109/LGRS.2019.2914432.

Xie, T., Zhang, W.K., Yang, L.N., Wang, Q.P., Huang, J.J. and Yuan, N.C. (2018). Inshore ship detection based on level set method and visual saliency for sar images, *Sensors* **18**(11): 3877, DOI: 10.3390/s18113877.

Xiong, B., Huang, X.H. and Wang, M. (2021). Local gradient field feature contrast measure for infrared small target

detection, *IEEE Geoscience and Remote Sensing Letters* **18**(3): 553–557, DOI: 10.1109/LGRS.2020.2976208.

Yang, L.L., Yan, P., Li, M.H., Zhang, J.L. and Xu, Z.Y. (2022). Infrared small target detection based on a group image-patch tensor model, *IEEE Geoscience and Remote Sensing Letters* **19**: 1–5, DOI: 10.1109/LGRS.2021.3140067.

Yao, S.B., Zhu, Q.Y., Zhang, T., Cui, W.N. and Yan, P.M. (2022). Infrared image small-target detection based on improved FCOS and spatio-temporal features, *Electronics* **11**(6): 933, DOI: 10.3390/electronics11060933.

Yu, X., Xie, W. and Yu, J. (2022). A single image deblurring approach based on a fractional order dark channel prior, *International Journal of Applied Mathematics and Computer Science* **32**(3): 441–454, DOI: 10.34768/amcs-2022-0032.

Zhang, H., Zhang, L., Yuan, D. and Chen, H. (2018). Infrared small target detection based on local intensity and gradient properties, *Infrared Physics and Technology* **89**: 88–96, DOI: 10.1016/j.infrared.2017.12.018.

Zhang, K., Yang, K., Li, S.Y. and Chen, H.B. (2019). A difference-based local contrast method for infrared small target detection under complex background, *IEEE Access* **7**: 105503–105513, DOI: 10.1109/ACCESS.2019.2932729.

Zhang, W., Cong, M.Y. and Wang, L.P. (2003). Algorithms for optical weak small targets detection and tracking: Review, *Proceedings of 2003 International Conference on Neural Networks and Signal Processing, Nanjing, China*, pp. 643–647.

Linna Yang was born in 1991. She received her MS degree in information and communication engineering from the National University of Defense Technology, Changsha, China, in 2015. She is a lecturer with the College of Information and Communication, National University of Defense Technology, Wuhan, China. Her current research interests include computer vision, machine learning and image processing.

Tao Xie was born in 1990. He received his MS and PhD degrees in electronic science and technology from the National University of Defense Technology in 2015 and 2019, respectively. Currently he is a lecturer with the College of Information and Communication, National University of Defense Technology, Wuhan, China. His research interests include superpixel segmentation and target detection.

Mingxing Liu was born in 1986. He received his MS and PhD degrees in management science and engineering from the National University of Defense Technology, Changsha, China, in 2009 and 2013, respectively. Currently he is a lecturer with the College of Information and Communication, National University of Defense Technology, Wuhan, China. His research interests include big data analysis and image processing.

Mingjiang Zhang was born in 1988. He received his MS degree in military equipment from the National University of Defense Technology, Xi'an, China, in 2017. He is a lecturer with the College of Information and Communication, National University of Defense Technology, Wuhan, China. His current research interests include computer vision, machine learning and target detection.

Shuaihui Qi was born in 1994. He received his MS degree in control sciences and engineering from the National University of Defense Technology, Changsha, China, in 2018. He is a lecturer with the College of Information and Communication, National University of Defense Technology, Wuhan, China. His present research interests include face detection, object detection, and semantic segmentation.

Jungang Yang was born in 1973. He received his MS and PhD degrees from the Institute of Communication Engineering, Xidian University, Xi'an, China, in 2003 and 2008, respectively. He is currently a professor with the College of Information and Communication, National University of Defense Technology, Wuhan, China. His current research interests include artificial intelligence security, intelligent combat, and research of unmanned platform.

Received: 17 April 2022
Revised: 11 September 2022
Accepted: 9 November 2022